JOURNAL OF MATERIALS SCIENCE **38** (2003) 1–7

Defect-free sintering of two material powder injection molded components

Part II *Model*

P. SURI, D. F. HEANEY, R. M. GERMAN*
Center for Innovative Sintered Products, 147, Research West, The Pennsylvania State University, University Park, PA 16801-6809, USA
E-mail: rmg4@psu.edu

A defect-free, two-material component can be obtained via co-sintering by suitably altering the powder characteristics or compositions, as demonstrated in Part I. In this paper, a model to ascertain the suitability of material systems to be co-sintered without defects such as delamination or interface pores is presented. The model is based on the management of the stress induced due to the difference in shrinkage and an analysis of the *in situ* strength of the weaker material during sintering. Tool steel in combination with stainless steel admixed with boron and Fe-2Ni admixed with boron are two systems used to validate the model. The predictions of the model are in good agreement with the observations. © *2003 Kluwer Academic Publishers*

1. Introduction

Particulate material processing techniques such as tape casting, compaction, and powder injection molding are used to produce functionally graded materials that find several applications such as layered ceramics for electronic applications, graded cutting tools, or cost-effective components. Sintering of the multi-component system is the most important step, since defects such as cracks, delamination, and interface porosity form during sintering. Defects due to difference in sintering kinetics arising from a difference in green density [1], particle characteristics [2], or powder composition [3, 4] have been documented. Further, the nature of the stress, that is, tensile or compressive, contributes to the above-mentioned defects and is dependent on the geometry of the green bodies. Few models have been proposed to account for the flaw generation during sintering of ceramic systems. A brief discussion on these models is given in the next section.

The present study aims at identifying the criteria for defect-free sintering of two-material system by considering the variation in the *in situ* strength of the materials as compared with the stress induced due to the difference in sintering shrinkage. Success of a two-material injection molding process depends on the formation of a defect-free and distortion-free component with a compatible interface between the materials. Compatibility in the present case refers to the chemical/metallurgical compatibility. For example, systems such as gold and glass or iron and alumina do not have any solid solubility. Consequently, a chemical or metallurgical bond is not possible even though a successful two-material component can be produced. In those cases, the strength of the interface is derived from residual thermal stresses. We consider systems that exhibit some degree of solid solubility. Further, it is assumed that defects are generated during the initial stage of sintering where the material is weakest. The resulting criteria are useful to evaluate the suitability of the two-material system, but are not meant to be design guidelines. Further, the conditions elucidated here are for the initial stage sintering only and do not explicitly consider distortion or warpage—which is largely influenced by the geometry of the component and the ensuing stress state.

2. Model

The criteria for sintering a two material system are dictated by the difference in the sintering shrinkage and the thermal expansion of the powders. An improper combination of these parameters can result in distortion or cracking [3–5]. Previous studies have recognized that a close match of the sintering shrinkage is essential to avoid defects and distortion during sintering [2–5]. Few models have been proposed to predict the distortion and defect formation during sintering of ceramic-ceramic or metal-ceramic systems [6–11]. However, the predictive abilities of these models is limited due to the formulation or underlying assumptions such as:

1. Elastic behavior without considering the effects of porosity: The assumption of elastic behavior is valid for ceramic systems at room temperatures. However, during sintering, the deviation from elastic behavior is observed at temperatures as low as 200°C [6]. Bordia

*Author to whom all correspondence should be addressed.

and Jagota [7] and Jagota and Hui [12] formulate the conditions for cracking during constrained sintering which are applicable only to elastic films with a weak interface [12]. Further, the parameters such as the uniaxial viscosity and the stress intensity factor are not a constant during sintering, but change with the microstructure, especially with the porosity. Thus, elastic models based on bulk properties can give erroneous results. Sintering of powder compacts is best described by considering plastic or viscous deformation formulations [6].

2. Failure criteria based on sintering stress formulations [3, 6, 9, 10, 13]: In principle, formulations based on constitutive equations for sintering are applicable to all materials using the generalized viscous models. However, the failure criteria based on sintering stress fails to yield the desired predictions [6] and is not an appropriate approach. Sintering stress is defined as stress from interfacial energies acting over curved surfaces [14]. Sintering stress is a mechanical equivalent of a difference in chemical potential. A difference in chemical potential arises due to a difference in the curvature, providing the driving force necessary for the densification and neck formation between the particles. However, it does not reflect the strength of the material. For example, it is possible for different material systems such as iron, bronze and alumina to have the same sintering stress (by suitably altering the particle characteristics), while the *in situ* strength of compacts of the compacts are vastly different.

3. Failure due to the effect of thermal stresses: A vast majority of finite element models analyze the interface stability of multi-component laminates under the action of residual thermal stresses. These models consider the effect of (elastic) thermal stress on crack generation and propagation. The assumption of such models is the presence of a defect-free laminate, with failure occurring during cooling as a result of the stresses generated due to thermal expansion mismatch. Such a condition is valid in cases where external pressure is applied to avoid failure during sintering. During free sintering (i.e., sintering in the absence of externally applied pressure), failure occurs during heating [3, 4, 8]. Hence models that consider the effect of difference in thermal expansion coefficient during cooling do not address the true cause of failure.

For tow material PIM components, damage is most likely to occur during the heating cycle and in the initial stage of sintering since the material is the weakest at this stage [8]. Further, plastic or viscous material behavior has to be considered to describe the stress state of the compact. Our model proposes that sintering of a defect-free two-material component can be achieved if the stress due to the difference in shrinkage during sintering does not exceed the *in situ* strength of the weaker material. A corollary is that a defect-free co-sintering can be realized if the difference in shrinkage of the tow materials does not exceed the failure strain of the weaker material. In what follows, the formulations for *in situ* strength and the stress due to shrinkage differences are presented.

3. *In situ* strength

Below the temperatures where diffusional phenomena are inactive, the powder compact is fragile and retains its shape either due to the binder or mere interparticle frictional forces. With an increase in temperature, the powder compact develops its strength because of neck formation (bonding between contacting particles). The strength of the powder compact gradually increases as interparticle necks grow, to the point where the material undergoes thermal softening. Such a variation in the *in situ* strength (σ_i) of a powder compact is a function of its material properties, particle size, relative density of the compact, and the neck size is given as [15]:

$$\sigma_i = \sigma_0 g(T) \frac{N_c \rho_s}{k\pi} \left(\frac{X}{D}\right)^2 \tag{1}$$

$$N_c = 14 - 10.3(1 - \rho_s)^{0.38} \tag{2}$$

$$\rho_s = \frac{\rho_g}{\left(1 - \Delta L/L\right)^3} \tag{3}$$

where, σ_0 is strength of the bulk material at room temperature, ρ_s is the fractional sintered density, ρ_g is the fractional green density, k is the stress concentration factor, X is the neck size, D is the particle diameter, N_c is the coordination number, $\Delta L/L$ is the shrinkage, and $g(T)$ is a normalized function describing the temperature dependence of the bulk strength.

Densification is not essential for a material to strengthen—surface diffusion promotes neck growth without densification and leads to an increase in the compact strength. Hence, the above phenomenological model, especially suited to estimate the *in situ* strength of a powder compact during the initial stages of sintering, is considered over other empirical models [16–18]. From Equation 1, the relative *in situ* strength depends on the inherent strength of the material and the neck growth during sintering. Thus, during co-sintering, the two materials that densify at different rates differ in their *in situ* strength. The material with lower *in situ* strength is referred to as a weaker material. Stress induced due to difference in sintering shrinkage.

In principle, an elastic-viscoplastic model best describes the deformation behavior of the powder compact. However, there are few models dealing with the elastic-viscoplastic constitutive relationships for porous materials [19–21]. The applicability of these models is involved with a need to determine additional material parameters to account for the viscous deformation. Further, the 'state' of the two-material compact, that is porosity, pore morphology, neck size, and connectivity varies during sintering requiring the determination of the temperature variation of the material parameters used in the constitutive relations. Experiments on the viscoplastic behavior of porous bronze and iron show that the strain rate sensitivity decreases with porosity [22]. Also, the time dependant creep deformation is negligible compared to the densification rate under the non-isothermal conditions operative during the initial stages of densification [23, 24]. Hence, the stress-state during early sintering is described by considering plastic deformation of the material.

Elasto-plastic behavior of many engineering alloys, including porous sintered metals, is described by various empirical relationships such as Ludwik's equation [25, 26], Hollomon's equation [27] or the Ramberg-Osgood equation [28]. These equations have been applied to sintered materials, predominantly ferrous alloy systems [25–27]. Here, we will utilize the Ramberg-Osgood equation to determine the stress induced due to a difference in the shrinkage during sintering, σ_s, given as:

$$\varepsilon = \varepsilon_e + \varepsilon_p = \frac{\sigma_s}{E} + \left(\frac{\sigma_s}{H}\right)^{\frac{1}{n}} \tag{4}$$

where, E is the modulus of elasticity, n is the strain-hardening exponent, ε is the true strain, ε_e is the elastic strain, ε_p is the plastic strain, and H is a constant, referred to as strength coefficient or plastic modulus.

For a fully dense material (superscript 0 refers to non-porous, bulk material),

$$\sigma = H^0 \varepsilon^n \tag{5}$$

$$\frac{d\sigma}{d\varepsilon} = nH^0 \varepsilon^{n-1} \tag{6}$$

By definition, at $\sigma = \sigma^0_{UTS}$, $\varepsilon = n$. Thus,

$$H^0 = \frac{\sigma^0_{UTS}}{n^n} \tag{7}$$

For a porous material [16]

$$\sigma_y = \sigma^0_y \frac{1-\theta}{k} \tag{8}$$

$$\sigma_{UTS} = \sigma^0_{UTS} \frac{1-\theta}{1+\alpha(k-1)\theta} \tag{9}$$

where, α is a constant, k is the stress concentration factor, and subscripts Y and UTS indicate yield and ultimate tensile strength. Further, from [26]

$$\frac{\sigma_y}{\sigma^0_y} = \frac{H}{H^0} \tag{10}$$

Thus, from Equations 7–10, the plastic modulus can be estimated by materials properties such as tensile strength (σ_{UTS}), fracture strength (σ_f) and fracture ductility (ε_f) as:

$$H = \frac{\sigma^0_{UTS}}{n^n} \frac{1-\theta}{k} \tag{11}$$

for a material undergoing plastic deformation with necking, and

$$H = \frac{\sigma_f}{\varepsilon_f^n} \frac{1-\theta}{k} \tag{12}$$

for a material undergoing plastic deformation without necking. Substituting Equation 11 in Equation 2 and neglecting the elastic deformation, we have

$$\varepsilon \approx \left(\frac{\sigma_s}{H}\right)^{1/n} = n\left(\frac{\sigma}{\sigma^0_{UTS}}\right)^{1/n} \left(\frac{k}{1-\theta}\right)^{1/n} \tag{13}$$

In the limiting case of $\theta \to 0$, Equation 13 reduces to $\varepsilon = n$ for $\sigma = \sigma_{UTS}$. Finally, from Equation 11, the strain-hardening rate ($d\sigma/d\varepsilon$) for the porous material shows the expected inverse dependence on porosity [26].

Hence, the condition for a defect-free two-material injection molded component can be represented as:

$$\sigma_i > \sigma_{se} \tag{14}$$

where, σ_i is the *in situ* strength of the weaker material (material with lower strength) and σ_{se} is the (engineering) stress induced due to the difference in shrinkage of the weaker material. The *in situ* strength of the interface is probably a more rigorous criterion. However, using the *in situ* strength of the weaker material is rationalized as follows: Consider Fig. 1, which gives a schematic of the various conditions that are possible for two materials A and B. If the *in situ* strength of material A is less than that of the interface and material B, then failure is expected in material A as shown in case (a). Case (c) is similar to (a) in that the *in situ* strength of material B is less than material A. If the strength of the interface is similar to that of either A or B as depicted in

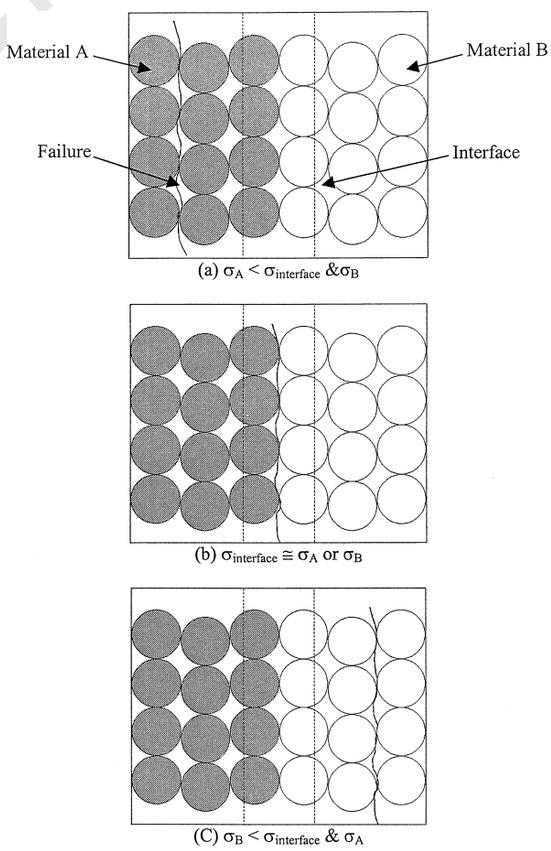

Figure 1 Schematic illustrating various scenarios of failure to justify the assumption of using the *in situ* strength of the weaker material as failure criteria.

TABLE I Functional dependence of material and geometry properties on temperature and porosity

Material property	$g(T)$	$h(\theta)$
E	$e^{\frac{-Qa}{RT}}$	$f(\theta) = (1-2\theta)\cdot(1+4\theta^2), 0 \le \theta \le 0.3$ $f(\theta) = (1-\theta)^2, 0.3 \le \theta \le 0.9$ [36]
σ_{UTS}	$\frac{a}{1+\exp(\frac{T-b}{c})}$	$\frac{\sigma_{0,UTS}}{k}$ [20]
n	Constant	Constant
k	—	$\exp(0.0946(\ln(\frac{X}{8D}))^2 + 0.1746\ln(\frac{X}{8D}) + 0.4576)$ [15, 37]

Where, Qa is the activation energy, R is the universal gas constant, $\sigma_{0,UTS}$ is the bulk tensile strength at room temperature, T is the absolute temperature, k is the stress concentration factor and a, b, c, d are constants.

Case (b), then the failure could occur at the interface or within one of the materials with equal probability. The assumption would lead to an over estimation of the *in situ* strength only if the strength of the interface is less than either material. However, such a situation is not anticipated as we assume compatibility between the materials (an alloy of A and B will have strength higher that either A or B).

The mechanical properties used in equations viz., E, H, σ_{UTS}, n, ε_f, are a function of temperature and porosity, parameters that have to be taken into consideration for accurate predictions. Assuming a separation of effects, the functional dependence of these material properties on temperature and porosity can be expressed as:

$$F(T,\theta) = F_0 g(T) h(\theta) \quad (15)$$

Au: Eq no. 15 ok as placed.

where, F_0 is the property of the bulk material at room temperature, T is the temperature and θ is the porosity. The functional dependencies used for calculation in the present work are listed in Table I.

4. Model verification and discussion

To determine the *in situ* strength of the material, one has to establish the evolution of neck size and density during sintering. Numerical simulation of the sintering process enables the prediction of these quantities. Calculations were realized via computer simulation considering the multiple transport mechanisms that occur simultaneously during sintering, viz., surface diffusion, grain boundary diffusion, and volume diffusion. Details on the formulations of the model and computation method are given in [15]. The material parameters for the simulations were adjusted such that the neck size ratios obtained from fractured surfaces are in close agreement with the numerical results and are given in Appendix 1. The variation in the neck size ratio of the compacts with temperature for M2 tool steel, 316L-0.5 wt% B stainless steel, and Fe-2 wt% Ni-0.5 wt% B is given in Fig. 2. The sintering cycle employed for the simulation was a heating rate of 5°C/min to 500°C for one hour, 5°C/min to 1000°C for one hour with a fractional green density of 60%. The figure shows that an increase in the sintering temperature and time promotes interparticle neck growth. Further, the neck size is larger for Fe-2Ni-0.5B, which is expected because of

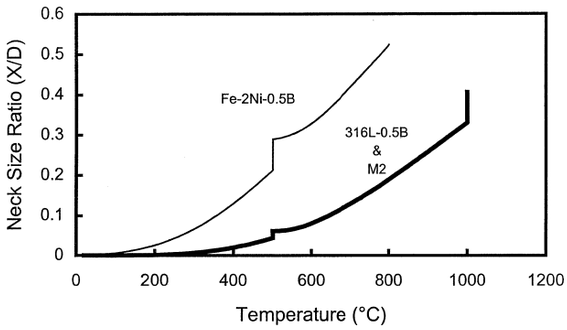

Figure 2 Simulated results of neck size evolution with temperature for steel powders with a green density of 60% sintered at 5°C/min to 500°C for one hour, 5°C/min to 1000°C. Particle sizes of 316L, Fe2NiB, and M2 and 10, 4, and 18 μm, respectively.

the higher shrinkage (5% at 800°C) and hence a lower activation energy for diffusion, compared to M2 and 316L-0.5B.

Fig. 3a–c shows the variation in the shrinkage with temperature obtained from simulations and a

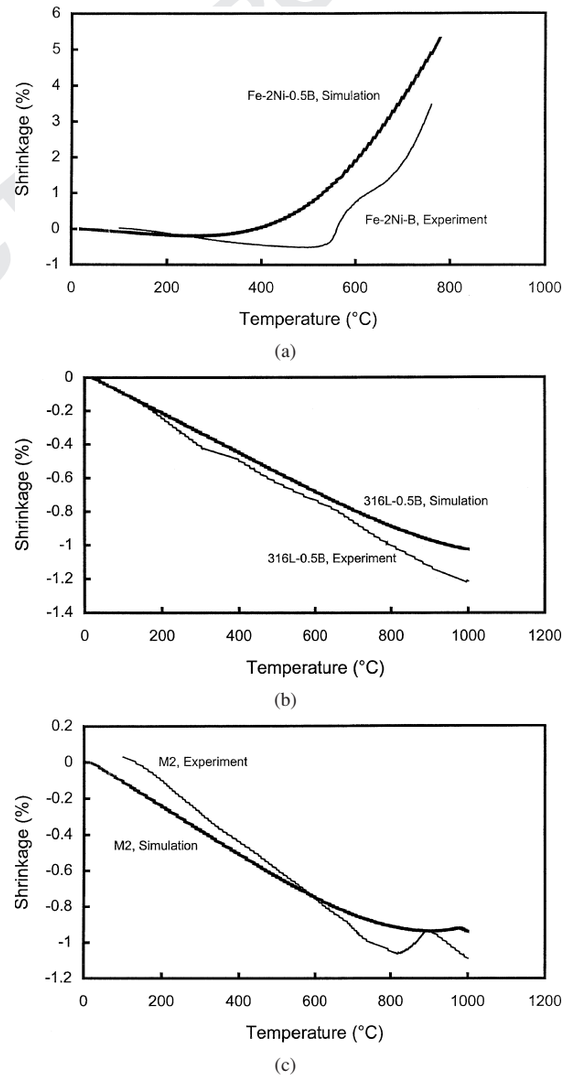

(a)

(b)

(c)

Figure 3 Variation in the sintering shrinkage with temperature obtained from simulations and comparison with experiments for (a) Fe-2Ni-0.5B, (b) 316L-0.5B, and (c) M2 tool steel.

comparison with the experimentally observed shrinkage. The experimental results and numerical simulations for M2 and 316L-0.5B are in close agreement, while simulation results over predict the shrinkage in the case of Fe-2Ni-0.5B. This is due to (i) the limitation of the model to consider dimensional changes due to phase transformation, and (ii) pre-processing of the samples prior to determining the shrinkage using dilatometry. As detailed in Part I [4], the compacts used for dilatometry were debound and presintered to remove the polymers and impart handling strength. The Fe-2Ni-0.5B compacts were debound and presintered at 500°C. Hence, these specimens exhibit thermal expansion up to 500°C and begin to densify at that point. Hence, the simulation results and the experiments in the case of Fe-2Ni-0.5B are expected to differ. The compacts of M2 and 316L-0.5B, on the other hand, do not exhibit a significant sintering shrinkage below 1000°C. Neck growth is observed for M2 and 316L-0.5B with the absence of sintering shrinkage, indicating the contribution of the surface diffusion.

The results from simulations were used to obtain the difference in shrinkage during sintering for Fe-2Ni-0.5B and 316L-0.5B with respect to M2 tool steel, and are given in Fig. 4. The difference in the shrinkage for 316L-0.5B with M2 is predominantly due to the difference in the coefficient of thermal expansion. This difference is approximately 0.14% at 500°C and about 0.23% at 800°C. On the other hand, the difference in shrinkage between Fe-2Ni-0.5B and M2 is 0.82% at 500°C and 5% at 800°C to the higher sintering densification of Fe-2Ni-0.5B.

The evolution of the *in situ* strength with temperature is given in Fig. 5. The compact strength increases during the initial stage sintering due to the inter-particle neck growth. A further increase in temperature, in the case of Fe-2Ni-0.5B promotes sintering shrinkage, decreasing the amount of porosity and contributes to a substantial increase in its strength. As sintering proceeds, the curvature of the neck decreases gradually reducing the effect of stress concentrators on its strength. The *in situ* strength of the material eventually decreases as the reduction in strength due to thermal softening exceeds the gain in strength due to neck growth [15, 29]. Fig. 5 shows that between M2 with 316L-0.5B material combination, 316L-0.5B has lower *in situ* strength and hence is the weaker material. For the M2 and Fe-2Ni-0.5B combination, M2 is weaker below 740°C, above which Fe-2Ni-0.5B has lower strength.

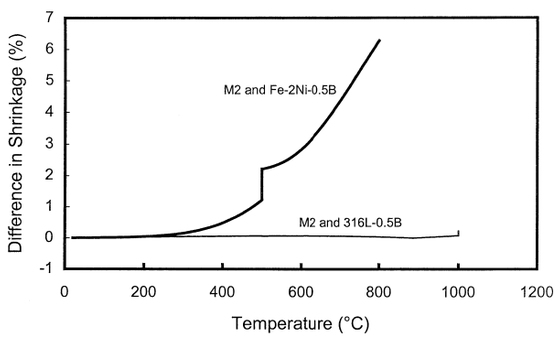

Figure 4 Difference in the shrinkage during sintering for M2 tool steel compact with Fe-2Ni-0.5B and 316L-0.5B systems.

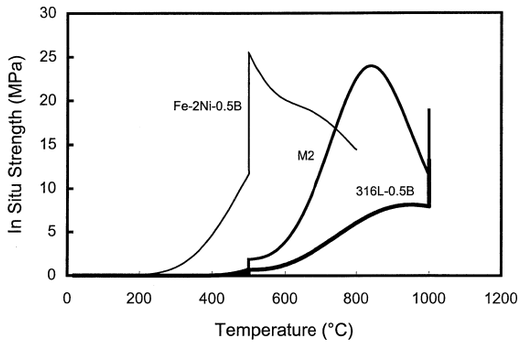

Figure 5 Evolution of the *in situ* strength of the steels with temperature. The strength of the compacts increases with an increase in temperature and time until the thermal softening exceeds the gain in strength due to neck growth.

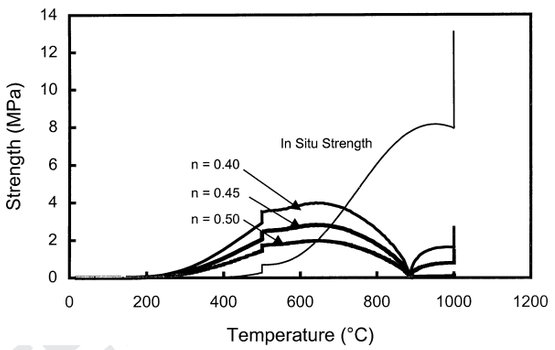

Figure 6 The variation in the stress induced due to the difference in shrinkage with temperature for M2 with 316L-0.5B. The figure shows the induced stress for different values of the strain hardening coefficient and a comparison with the *in situ* strength.

The variation in the stress induced due to the difference in shrinkage with temperature for M2 with Fe-2Ni-0.5B and M2 with 316L-0.5B is given in Figs 6 and 7. The material parameters and their functional dependence on temperature and porosity are given in Appendix 2. Fig. 6 shows that the stress induced in the M2 compact below 740°C is greater than the *in situ* strength by an order of magnitude, in agreement with the observation that this material combination exhibits defect during processing [4, 30]. Below 300°C, the induced stress is less than 5 MPa and much greater than the *in situ* strength of either M2 or Fe-2Ni-0.5B. However, it is very unlikely that these stresses would result in any defects. Cai *et al*. [31] observed particle rearrangement in the compact prior to the onset of sintering under externally applied pressures of up to 5 MPa. Hence, below 300°C, the small stresses on the compact that is essentially a collection of loose powders held together by a binder or interparticle friction, may contribute to particle rearrangement (or reorientation) rather than cause defects and failure. Based on this reasoning, it can be seen that the stress induced due to the difference in sintering shrinkage is less than 5 MPa for the M2 and 316L-0.5B system below 600°C. Above 600°C, the induced stress does not exceed the *in situ* strength of the compact. This is in accordance with the

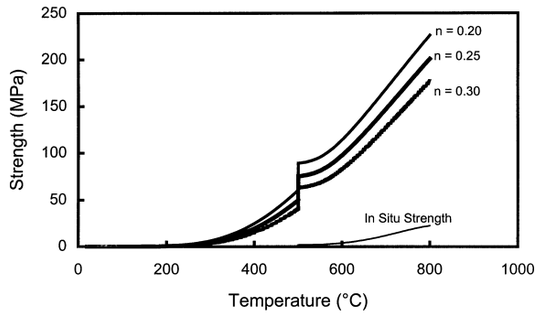

Figure 7 The variation in the stress induced due to the difference in shrinkage with temperature for M2 with Fe-2Ni-0.5B. The figure shows the induced stress for different values of strain hardening coefficient and a comparison with the *in situ* strength.

experimental observations that no sintering defects are observed for the M2 and 316L-0.5B system.

In reality, the strain hardening coefficient (n) depends on temperature, extent of cold working, and strain rate. Porosity has a negligible effect on strain hardening [26, 32]. In the present case, temperature is the dominant parameter, with a reported variation of ± 0.05 [33, 34]. Figs 6 and 7 show the effect of change in the strain-hardening coefficient. An increase in the strain-hardening coefficient decreases the induced stress; however, this variation does not affect the general conclusions regarding the defect formation, justifying the assumption of a constant strain hardening coefficient.

The difference in shrinkage behavior can be used to an advantage by an appropriate component design. For example, FeNiB can be molded around tool steel as the core, so that difference in sintering shrinkage does not lead to delamination or cracking. However, this imposes constraints on the material-system and design in that it cannot be used in complex geometries. Hence, in the context of powder injection molding as an enabling technology to fabricate near-net, complex shaped components, such a material combination does not yield a defect-free interface.

5. Conclusions

A model to predict defect-free sintering of two-material injection molded components is presented. The model compares the stress induced due to the difference in the sintering behavior of the two materials with the strength evolution of the interface during sintering. A defect-free component can be sintered if the induced stress does not exceed the *in situ* strength of the interface.

This model is unique in that it predicts defect formation in a sintered two-material system taking plasticity of the material into consideration. Further, the model provides a basis for alternatives in terms of tailoring the particle characteristics or processing conditions to obtain a defect-free two-material system.

The powder compact is weakest in the initial stage of sintering and this is the temperature range in which differences in shrinkage due to sintering or phase transformations can cause interface failure. Defects generated at these temperatures persist throughout the sintering cycle.

During initial stage sintering, neck growth occurs without significant densification. Neck growth contributes to a large gain in strength of the compact. At the end of the sintering cycle, the inherent strength of the material decreases and its ability to accommodate large deformations increases and the compact undergoes densification with less susceptibility to damage.

Acknowledgement

The authors wish to thank Lye-King Tan and Advanced Materials Technologies Pte Ltd, Singapore for supporting this effort.

Appendix 1: Material constants used to simulate neck size ratio and shrinkage during sintering. The sintering cycle used in the simulation was 5°C/min to 500°C for 1 h, 5°C/min to 1000°C for 1 h, 10°C/min to 25°C

	Fe-2Ni-0.5B (FeNiB)	316L-0.5B (316LB)	M2 Tool steel (M2)
Density (kg/m^3)	8020	8050	8000
Atomic volume (m^3)	7.98×10^{-30}	8.02×10^{-30}	8.02×10^{-30}
Volume diffusion frequency factor (m^2/s)	2×10^{-4}	4×10^{-5}	4×10^{-5}
Activation energy for volume diffusion (kJ/mol)	251	280	280
Surface diffusion frequency factor (m^2/s)	11	0.4	0.5
Activation energy for surface diffusion (kJ/mol)	239	250	215
Grain boundary diffusion frequency factor (m^3/s)	10^{-17}	2×10^{-13}	2×10^{-13}
Activation energy for grain boundary diffusion (kJ/mol)	128	167	167
Pre-exponential vapor pressure (MPa)	7.4×10^4	7.4×10^4	7.4×10^4
Activation energy for evaporation-condensation (kJ/mol)	340	340	340
Surface energy (J/m^2)	1.95	2	2.2

Appendix 2: Variation in the elastic modulus and strength of the steels with temperature used in the calculations [35]

Variation in the elastic modulus of austenitic steel with temperature

$$g(T) = \exp\left(\frac{111.94}{T} + 4.9044\right) R^2 = 0.96$$

Thermal Softening of Tool Steel

$$g(T) = \frac{1.02}{1 + \exp\left(\frac{T - 1101.78}{69.14}\right)}, R^2 = 0.97$$

Thermal softening for 316L

$$g(T) = \frac{0.9532}{1 + \exp\left(\frac{T-1003}{138.3}\right)}, R^2 = 0.983$$

Fe-2Ni-1B (approximated from the data for Fe-2Ni-0.7Cr)

$$g(T) = \frac{1.019}{1 + \exp\left(\frac{T-764.6}{112.5}\right)}, R^2 = 0.97$$

Fe-10Cr-0.5B (approximated from the data for Fe-9Cr-1.5Mo)

$$g(T) = \frac{1.064}{1 + \exp\left(\frac{T-787.7}{172.5}\right)}, R^2 = 0.97$$

References

1. C. A. BRUSH, *Amer. Ceram. Soc. Bulletin* **41** (1962) 799.
2. F. F. LANGE and M. METCALF, *J. Amer. Ceram. Soc.* **66** (1983) 398.
3. P. Z. CAI, D. J. GREEN and G. L. MESSING, *ibid.* **80** (1997) 1929.
4. D. F. HEANEY, P. SURI and R. M. GERMAN, Part I, Submitted to the Same Journal.
5. A. ZAVALIANGOS and Y. LI, in "Advances in Powder Metallurgy and Particulate Materials," edited by J. J. Oakes and J. H. Reinshagen (Metal Powder Industries Federation, Princeton, NJ, 1998) Vol. 2, p. 7.
6. P. Z. CAI, D. J. GREEN and G. L. MESSING, *J. Amer. Ceram. Soc.* **80** (1997) 1940.
7. R. K. BORDIA and A. JAGOTA, *ibid.* **76** (1993) 2475.
8. T. CHENG and R. RAJ, *ibid.* **72** (1989) 1649.
9. K. SHINAGAWA, in Proceedings of the 4th International Symposium on Functionally Graded Materials, edited by I. Shiota and Y. Miyamoto, Tsukuba, Japan, 1996, p. 69.
10. A. MAXIMENKO, O. VAN DER BIEST and E. OLEVSKY, *Inter. J. Fract.* **110** (2001) L9.
11. H. RIEDEL and T. KRAFT, Materials Science Forum, Vol. 308–311, 1999, in Proceedings of the 5th International Symposium on Functionally Graded Materials, edited by W. A. Kaysser, Dresden, Germany, 1998, p. 1035.
12. A. JAGOTA and C. Y. HUI, *Mech. Mater.* **11** (1991) 221.
13. J. KANTERS, U. EISELE and J. RODEL, *J. Amer. Ceram. Soc.* **84** (2001) 2757.
14. R. M. GERMAN, in "Sintering Theory and Practice" (Wiley-Interscience Publication, John Wiley and Sons, New York, NY, 1996) p. 76.
15. X. XU, P. LU and R. M. GERMAN, *J. Mater. Sci.* **37** (2002) 117.
16. R. HAYNES, *Rev. Def. Behav. Mater.* **3** (1981) 1.
17. H. DANNIGER, G. JANGG, B. WEISS and R. STICKLER, *Powder Met. Intl.* **25** (1993) 111.
18. E. NAVARA and B. BENGTSSON, *Intl. J. Powder Met. Powder Tech.* **20** (1984) 33.
19. M. HAGHI and L. ANAND, *Mech. Mater.* **13** (1992) 37.
20. C. GEINDREAU, D. BOUVARD and P. DOREMUS, *Euro. J. Mech. Solids* **18** (1999) 597.
21. M. B. RUBIN, O. Y. VOROBIEU and L. A. GLEN, *Intl. J. Solids Struct.* **37** (2000) 1841.
22. B. WANG, J. R. KLEPACZKO, G. LU and L. X. KONG, *J. Mater. Proc. Tech.* **113** (2001) 574.
23. R. RAJ and R. K. BORDIA, *Acta Metall.* **32** (1984) 1003.
24. M. GASIK and B. ZHANG, *Comp. Mater. Sci.* **18** (2000) 93.
25. U. LINDSTEDT, B. KARLSON and R. MASINI, *Intl. J. Powder Met.* **33** (1997) 49.
26. E. S. PALMA, *J. Brazilian Soc. Mechan. Sci.* **29** (1997) 72.
27. N. E. DOWLING, in "Mechanical Behavior of Materials: Engineering Methods for Deformation, Fracture and Fatigue," 2nd ed, (Prentice Hall, New Jersey, 1998) p. 565.
28. L. BERTINI, V. FONTANARI and G. STRAFFELINI, *Trans. Amer. Soc. Mechan. Eng.* **120** (1998) 248.
29. G. A. SHOALES and R. M. GERMAN, *Met. Mater. Trans.* **29A** (1998) 1257.
30. A. PEST, F. PETZOLDT, H. EIFERT, G. VELTL and T. HARTWIG, in "Advances in Powder Metallurgy and Particulate Materials," edited by T. M. Cadle and K. S. Narasimhan (Metal Powder Industries Federation, Princeton, NJ, 1996) Vol. 5, p. 19.171.
31. P. Z. CAI, G. L. MESING and D. L. GREEN, *J. Amer. Ceram. Soc.* **80** (1997) 445.
32. U. LINDSTEDT and B. KARLSSON, Doktorsavhandlingar vid Chalmers Tekniska Hogskola (1998) Vol. 1375, p. 1.
33. S. LOU and D. O. NORTHWOOD, *J. Mater. Eng. Per.* **33** (1994) 344.
34. N. S. MISHRA, S. MISHRA and V. RAMASWAMY, *Met. Trans.* **20A** (1989) 2819.
35. "Engineering Properties of Steel," edited by P. D. Harvey (American Society of Metals, Metals Park, OH, 1982).
36. G. LU, G. Q. LU and Z. M. XIAO, *J. Porous Mater.* **6** (1999) 359.
37. W. D. PILKEY, in "Peterson's Stress Concentration Factors," 2nd ed. (John Wiley & Sons, New York, NY, 1997).

Received 10 March
and accepted 14 August 2003